A&A 527, A55 (2011)
DOI: 10.1051/0004-6361/201015213

Astronomy & Astrophysics

The Cygnus Loop: a weak core-collapse SN in our Galaxy

A. Preite Martinez[1,2]

[1] INAF/IASF-Roma, via del Fosso del Cavaliere 100, 00133 Roma, Italy
e-mail: andrea.preitemartinez@iasf-roma.inaf.it
[2] Observatoire de Strasbourg, 11 rue de l'Université, 67000 Strasbourg, France

Received 15 June 2010 / Accepted 8 December 2010

ABSTRACT

Context. The Cygnus Loop is thought to be the result of a core-collapse supernova (SN) explosion in the cavity formed by the wind of the progenitor star. Since then the shock has run through the low-density cavity, hit the cavity wall, and it is now running into a denser environment.
Aims. We test the consistency of the global parameters of the remnant (as derived at the cavity-cloud interface) with the observational scenario in the north-east (NE) sector of the remnant.
Methods. The test is performed with the help of a time-dependent spherically-symmetric hydrodynamical (HD) code using a smooth density distribution at the cavity-cloud interface.
Results. When the shock hits the wall of the cavity, the reflected perturbation is found not to be a shock wave but a strong compression wave. The reflected wave heats up the cavity at temperatures higher than those observed in the X-rays. We also find an outwardly decreasing temperature as observed in X-rays, but over a narrower radial interval. After crossing the wall of the cavity, the shock velocity in the cloud is not steady. Nonetheless, we find that the steady-state assumption usually made to fit the line emission of Balmer-dominated non-radiative filaments (NRFs) can be rather accurate (shock velocity variations <3%) if the integration time of the post-shock structure is shorter than ∼200 y, the shock is not too close to the wall and the cloud was not shocked more than ∼1100 yr ago.
Conclusions. We propose a revision of the parameters of the cavity-wall scenario, assuming as a constraint the approximate steadiness of the shock velocity in the cloud. With the revised set of parameters, the values of the temperature in the hot cavity are in closer agreement with observations. At the adopted distance of 540 pc, we find an explosion energy $E_0 \simeq 6$–8×10^{49} erg, consistent with previous determinations of E_0 once scaled to the adopted distance. We also determine lower and upper limits of 0.1 and 2.6×10^{50} erg. This very low value of E_0 suggests an electron-capture explosion of an ∼8–10 $M_\odot$ progenitor, and makes the SN of the Cygnus Loop the weakest known core-collapse SN in the Galaxy.

Key words. ISM: supernova remnants – ISM: individual objects: Cygnus Loop – supernovae: general – hydrodynamics – shock waves

1. Introduction

The Cygnus Loop is a middle-aged supernova remnant (SNR), which is well-studied at radio, optical, UV, and X-ray wavelengths, that is roughly circular with a radius of ≃1.4 deg (Levenson et al. 1998). On the basis of the proper motion measurements of Balmer-dominated filaments in the NE, it is relatively nearby (540 pc according to Blair et al. 2005, with an upper limit of ∼580 pc given by Blair et al. 2009).

Many authors (McCray & Snow 1979; Braun & Strom 1986; Levenson et al. 1997) have found rather different shock velocities and densities for the unperturbed medium from optical/UV and X-ray observations. X-ray emission close to the rim of the remnant appears to come from plasma with temperatures in the range 0.2−0.3 keV (Uchida et al. 2009) (corresponding to shock velocities on the order of 350−450 km s^{-1}) and densities of ∼0.1 cm^{-3} (or ∼0.2 cm^{-3}, according to Raymond et al. 2003; Sankrit et al. 2010), while the main shock seems to run at a much lower velocity (Long et al. 1992, hereafter L92) through a medium of higher density (∼1−2 cm^{-3}). This is particularly evident in the NE limb of the Cygnus Loop, one of the brightest regions of the remnant. These authors have suggested that the observational scenario is consistent with the hypothesis that the explosion of the SN that produced the Cygnus Loop occurred within a pre-existing bubble, shell, or cavity generated by the wind of the progenitor star, that the shock has already run through the wall of the cavity, and that it is now interacting with a surrounding cloud of denser material.

Balmer-dominated filaments, detected in the optical and the UV (Danforth et al. 2000), are supposed to trace the position of the main shock. They have been studied with the help of non-radiative steady-state shock models (L92; Raymond et al. 1983; Hester et al. 1994; Blair et al. 2005, just to quote work on the NE sector of the remnant). The derived values of the shock velocity vary in the range ∼130−210 km s^{-1}, concentrating around 180 km s^{-1}.

In their work on one of these filaments, Hester et al. (1994), hereafter HRB94, confirm the hypothesis of a cavity explosion and determine quantitatively the basic parameters of the remnant at the cavity-cloud interface, which is assumed to be a discontinuity. In their scenario, the remnant hit the cavity wall when its shock velocity was $V_S \simeq 450$ km s^{-1} (corresponding to a supposed post-shock temperature of ∼0.24 keV), the pre-shock density beyond the wall is ∼1.3 cm^{-3}, and the density jump at the cavity wall should then be 14 to ensure a transmitted shock of 180 km s^{-1}.

Observations of the remnant in the X-rays with *ASCA* (Miyata & Tsunemi 1999, 2001), *XMM-Newton* (Nemes et al. 2008; Katsuda & Tsunemi 2008), *Chandra* (Levenson et al. 2002; Katsuda et al. 2008a), and *Suzaku* (Miyata et al. 2007; Katsuda et al. 2008b; Uchida et al. 2009) are all consistent with the cavity explosion scenario. They also show that the (line-of-sight averaged) temperature of the shocked gas decreases with the projected radius of the remnant (Nemes et al. 2008), and that the temperature just behind the wall of the cavity is only marginally lower (as can be deduced from Fig. 3 of Uchida et al. 2009) than the 0.24 keV used by HRB94.

The purpose of this work is to test the consistency of the global parameters of the remnant (as derived by HRB94 at the cavity-cloud interface) with the observational scenario in the NE sector of the remnant, in particular the X-ray observations. We also test the assumption made when deriving the input parameters, i.e. the supposed steadiness of the post-shock flow.

In Sect. 2, we use the parameters proposed by HRB94 as boundary and initial conditions for a time-dependent 1-D spherically symmetric HD model, and assume for the wall of the cavity a smooth density distribution. As a byproduct, we can estimate the total explosion energy E_0 of the Cygnus Loop SN. The discussion of the results and the proposition of a revised set of parameters for the HD model follow in Sects. 3.1–3.4. The explosion energy of the SN and the implications for its progenitor star are discussed in Sect. 3.5.

2. The 1-D HD model

The evolution of a SN shock in the cavity generated by the wind of the SN progenitor was described by Dwarkadas (2005) using a 1-D HD code, and by Dwarkadas (2007) in 2-D. The context of these studies was not that of the Cygnus Loop: the progenitor was supposed to be a Wolf-Rayet star of 35 $M_\odot$, and at the moment of the explosion the radius of the wind-generated bubble was ∼80 pc. According to Miyata & Tsunemi (1999), the mass of the progenitor of the Cygnus Loop SN is only ∼15 $M_\odot$ (or lower, because they assume a distance d of 770 pc), and the radius of the bubble is on the order of 18(d/770) pc.

A global model of the Cygnus Loop was presented by Falle & Garlick (1982). They used an axisymmetric 2-D HD model to show that high velocities in the Cygnus Loop can be explained by a breakout taking place in a direction roughly towards us. Many authors have modeled the emission of radiative and non-radiative regions of the remnant. They have used a steady-state approximation to the time-dependent HD problem to model the post-shock structure of the flow, which is assumed to be steady. For an analysis of this method and references, we refer to the short review of Preite Martinez (2009).

In this paper, we use a 1-D spherically symmetric HD code. The use of a 1-D code is sufficient to test the consistency of the global parameters of the remnant with the observational scenario. One should bear in mind though that the test is only valid for the NE sector of the remnant, where the input parameters have been derived.

The 1-D spherically symmetric HD code was described in Preite-Martinez (1981) and in Fusco-Femiano & Preite-Martinez (1984). The standard system of partial differential equations is solved following the "characteristics" integration schema described by Falle (1975). In this schema, the shock is a discontinuity and the Rankine-Hugoniot relations are used. The HD equations are coupled to the time-dependent ionization structure of 15 of the most abundant elements, and the corresponding cooling of the ionic species is taken from the CHIANTI database (Dere et al. 1997). The ambient medium is assumed to be ionized (the relative concentration of the first degree of ionization of all elements is set to 1), warm (T = 10 000 K), and to have a weak transversal magnetic field of 0.1 μG (value also used by L92). In any case, the ionization structure of the ambient medium has negligible effects on the HD structure of the remnant.

The HRB94 scenario constrains the boundary and initial conditions of the model (that we call the reference model). As an initial condition, we assume a Sedov-Taylor similarity solution (Sedov 1959) characterized by an explosion energy E_0, expanding adiabatically in a medium of constant density n_0 up to the wall R_w of the cavity. In the cavity, the remnant is indeed adiabatic: we see in Sect. 3.3 that the cooling time is $>10^5$ yr.

The assumption that the density distribution is constant within the cavity ($n(r) = n_0$) is probably a rather rough approximation. Dwarkadas (2007) demonstrated that the density distribution in a wind-generated cavity can be highly variable, even by orders of magnitude. Although the results of his work cannot be simply scaled down to the case of the Cygnus Loop, it seems reasonable to expect some degree of variability of the density in the cavity. The simplest way out is then to take a heuristic approach, considering n_0 as the particular average value of $n(r)$ that reproduces in the proximity of the cavity wall the same values of the shock parameters as those given by an evolution with a variable $n(r)$. This assumption allows us to use the adiabatic equations to derive the parameters of the shock just before it hits the wall of the cavity.

To evaluate E_0 (or $E_{51} = E_0/10^{51}$ erg), we can then use the Sedov-Taylor equations describing the evolution of the shock, namely $R_S \propto \zeta^{0.2}\, t^{0.4}$ and $V_S \propto \zeta^{0.2}\, t^{-0.6}$, where R_S and V_S are the radius and velocity of the shock, t is the age of the remnant, and $\zeta = E_{51}/n_0$.

If we consider that the wall of the cavity at present times must coincide with the edge of the radiative region, at a radius of ∼84′ = 13.19 (d/540) pc (Levenson et al. 1998), and that after hitting the wall the shock could be ∼30″ up to ∼2′ further away, we can estimate the position of the wall at the time it was hit by the shock to be ≲13 pc.

Eliminating $t \propto R_S/V_S$ from the above Sedov-Taylor equations, we get $\zeta \simeq 2 \times 10^{-5}\,(V_S/100\,\mathrm{km\,s^{-1}})^2\,(R_S/\mathrm{pc})^3$. We can evaluate ζ just before the wall, using the values V_S = 450 km s^{-1} and R_S = 13 pc. Thus, we have $\zeta \simeq 0.89$ and then $E_{51} = n_0\zeta \simeq 0.08$. The implications of this low value of the explosion energy will be discussed in Sect. 3.5.

To complete the up-stream boundary conditions, we need to define the density distribution of matter outside the cavity, which we refer to as the cloud although in our 1-D representation it is a shell, and at the cavity-cloud interface, which we call the wall. HRB94 assume for simplicity that the interface is a discontinuity, but suggest that it is more likely that "the shock is running up a steep density gradient at the edge of the cavity". For the density distribution of the cloud, we then assume the form $n(r) = n_c f(r)$ with $n(r) \geq n_0$, where

$$f(r) = \frac{a^3}{(a^2 + (R_c - r)^2)^{3/2}}, \quad (1)$$

R_c is the radius of maximum density n_c of the cloud, and n_0 is the constant density of the cavity. We can have different slopes before and after R_c assigning different values to a, i.e. $a = a^-$(for $r < R_c$) and $a = a^+$(for $r > R_c$). For the slope at the edge of the cavity, we tested different values of the parameter a^- in the range 0.1–0.001 pc, eventually adopting a value of 0.01 pc. A slope with this value of a^- is well described by the 300 mesh points grid used for the model.

Table 1. Relevant input parameters of the 1-D HD models.

Model:	Reference	Revised
E_{51}	0.08	0.06
n_0 (cm^{-3})	0.09	0.09
n_c (cm^{-3})	1.26	1.0
R_c (pc)	13.0	12.8
a^- (pc)	0.01	0.01
a^+ (pc)	1000	0.5

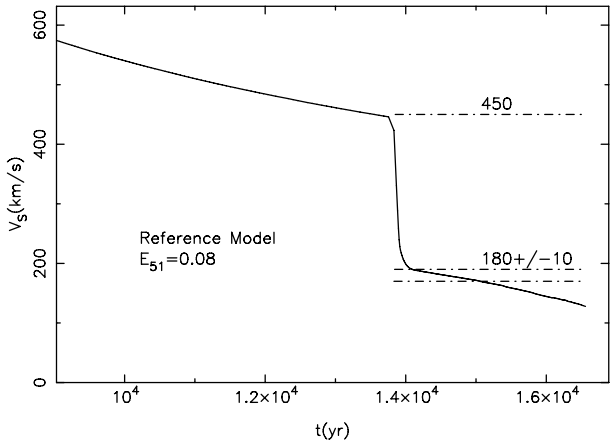

Fig. 1. Time evolution of the shock velocity V_S in the reference model (E_{51} = 0.08). Dot-dashed lines are drawn at V_S = 180 ± 10 and 450 km s^{-1}.

Although the edge of the cavity is not treated as a discontinuity, in the following we will continue to use the term "wall". We note also that with the formalism of Eq. (1), R_c is not the radius R_w of the wall, but rather $R_w \simeq R_c - a^-$.

In the second column of Table 1, we list the values adopted for the input parameters of the reference HD model. We have set a^+ to a very high value (1000 pc) to simulate a constant density distribution within the cloud.

3. Results and discussion

The reference model confirms the expected behavior of the shock at the cavity-cloud interface, as evaluated by HRB94. As can be seen in Fig. 1, just before hitting the cavity wall $V_S \simeq 450$ km s^{-1}, and after the wall V_S falls in the region marked in the figure by two dot-dashed lines drawn at 180 ± 10 km s^{-1}. Although this is what one would expect, given the densities before and after the wall, the radius of the wall, the impact velocity of the shock, and the total energy E_0, there are important features of the model that suggest a modification of the input parameters is necessary.

3.1. The temperature distribution

The first parameter that may need to be revised is the radial temperature distribution $T(r)$ of the reference model, shown in Fig. 2. Before the impact with the wall (see temperature distribution with label 1), $T(r)$ is in the correct range of observed temperatures e.g., 0.20–0.28 keV (Nemes et al. 2008; Uchida et al. 2009), at least in the outer regions behind the shock where the density is the highest. This is because of our choice of $V_S \simeq 450$ km s^{-1} when the shock hits the wall. Once the shock encounters the density increase at the wall, a compression wave is reflected downstream.

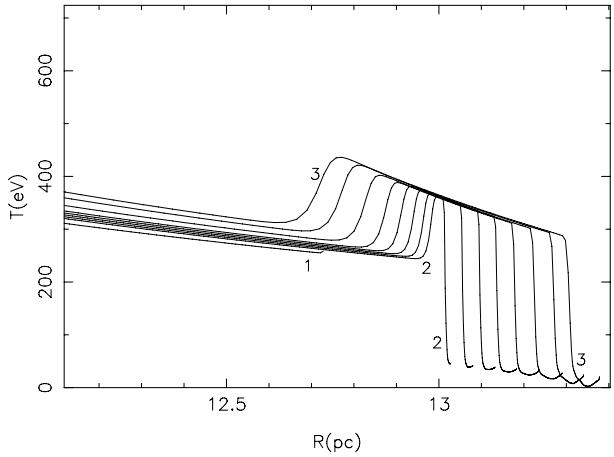

Fig. 2. The radial temperature distribution in the reference model at different times before and after hitting the cavity wall. Temperature T expressed in eV. Labels 1 to 3 refer to the specific times: (1) −723 yr, (2) +213 yr, (3) +2688 yr.

We note that with the present set of (HD and integration) parameters the reflected wave is not a shock wave. To test the physical conditions that could lead to the formation of a secondary shock, at each time step and for each grid point of the HD model, we extrapolate in the immediate future (few time steps) the characteristic curves C_+, C_- passing through each grid point, searching for a cusp. The presence of a cusp in a set of characteristic curves defines the onset of a shock. This method also provides an estimate of the (mass) coordinate and the time of onset of the shock, and its direction of propagation (up- or down-stream).

We tested different gradients (i.e. different values of $a = a^-$ in Eq. (1)) for the shape of the density distribution at the wall of the cavity: the reflection wave is a (downstream propagating) shock wave only in the case of a gradient that is considered as a discontinuity by the numerical program, i.e. when the passage from the cavity to the external cloud occurs within one single mesh interval of the Lagrangian grid. In the present model, with a Lagrangian grid that closely describes the adopted slope $a^- = 0.01$ pc, this happens for slopes with $a^- \lesssim 0.001$ pc. This value should not be over-interpreted: it only corresponds to the radial spacing of the grid at the mass coordinate of the wall. These tests were done at a constant density contrast cloud-cavity of 14. By assuming a constant $a^- = 0.01$ pc, we considered models with different density contrasts, from the 14 of the reference model up to a contrast of 30, 50, and eventually 140, but the reflected wave was always a compression not a shock wave.

Why do other HD models (e.g. Dwarkadas 2005) produce reflected shocks? It may be because of the way in which HD codes treat discontinuities and differentiate between a discontinuity and a steep gradient. As reported above, when our model hits a discontinuity a reflected shock is generated. The difference between the formation of a compression wave and the formation of a shock discontinuity is determined by testing the physical conditions. One could ask what sort of reflected wave is generated by models that treat discontinuities differently from ours, when they hit a steep gradient such as the one described by Eq. (1) and the parameters of Table 1.

The effect of the passage of the reflected wave is twofold: matter behind the shock is compressed and heated, and the slope of the radial temperature distribution changes from being almost constant to a steeper distribution. Nemes et al. (2008) reported a

~25% temperature decrease outwards over ~15% of the radius. In the present case, the relative temperature decrease is similar (~30%) but over a narrower region (~5% of the radius, see distribution (3) in Fig. 2). Uchida et al. (2009) showed the radial distribution of the emission measure in the NE sector of the remnant. In the present model, the values at the peak of the distribution of the emission measure near the border of the remnant are consistent with the observed values (of around 1.5×10^{20} cm^{-5}, although with ample variations as a function of age), but the width of the distribution is much narrower.

The comparison with information derived from X-ray data confirms that the shock has indeed hit a denser region, generating a wave that re-heats the post-shock flow. It also tells us that the relative temperature increase – depending on the assumed parameters of the wall/cloud – is the correct one, and that the reflected wave has traveled downstream for the time necessary to increase the temperature of a radial region by non-negligible extent. This means that the shock has not collided with the wall/cloud very recently but, according to the model, at least 2500−3000 yr ago, or even more, if we wish to explain the observed thickness of the re-heated region without drastic changes to the current scenario. Additional work is necessary at this point, both observationally – more precise radial temperature distributions at different azimuths in the NE sector – and in terms of modeling since the HD model of the cavity-wall scenario, as it stands, is unable to generate a region of increasing T inwards of the observed extent.

Although the relative temperature increase is consistent with the observed increase, at the time of observation (probably a few thousand years after the shock hit the wall) matter within the wall is no longer in the observed temperature range: as can be seen from the temperature distribution labeled (3) in Fig. 2, matter is a factor ~1.4 hotter (0.3–0.4 keV). To ensure that the temperature range is correct we need a shock that reaches the wall with a velocity lower by a factor $\sim\sqrt{1.4}$. As a consequence, keeping all other parameters constant (radius of the cavity, density in the cavity, shock velocity on the order of 180 km s^{-1} after the crossing of the wall), either the density jump at the wall or the explosion energy E_0 should be reduced by approximately the same factor (because $E_0 \propto V_S^2$).

3.2. The time evolution of V_S

The second parameter possibly needing revision is the time evolution of the shock velocity after the wall, within a constant density cloud. As can be seen form Fig. 1, V_S indeed lowers to ~180 km s^{-1}, but then continues decreasing, as it should do in a constant density medium. When the integration stopped, 2688 yr after hitting the wall, V_S was <130 km s^{-1} (V_S falls below 170 km s^{-1} after ~1100 yr).

The decrease in V_S with time has two important consequences. The first concerns the assumption of the steadiness of the post-shock flow in models of Balmer-dominated NRFs.

One standard assumption of the steady-shock approximation is that the upstream boundary conditions of the flow (e.g. ambient density, shock velocity) do not change significantly during the integration time t_i (the time necessary to build-up the steady flow to a linear extent $\sim t_i V_S/4$) of the post-shock downstream flow (see Cox 1972; Raymond 1979, for a definition of t_i). If we are interested in the emission due to the radiative cooling, the integration time must be shorter than the hydrodynamical timescale τ_{HD} (to approximate steadiness) but longer than the cooling timescale τ_c (for radiative cooling to take place). If we compute a non-radiative steady shock model, the integration time must again be shorter than τ_{HD} but also shorter that, or at most on the order of, τ_c. An additional constraint set by HRB94 for the NE sector of the Cygnus Loop is that the non-radiative steady flow has to extend for 0.5–2′. Considering that in a steady shock model with $V_S = 180$ km s^{-1} shocked matter is receding from the shock at $\sim 1/4 V_S = 45$ km s^{-1} and assuming that the average width of the non-radiative region is $1' = 0.157\,(d/540)$ pc, the shock is required to be steady and non-radiative for ~3400 yr.

The HD reference model tells us that at $V_S = 180$ km s^{-1} we have $\tau_c \simeq \tau_{HD} \simeq 900$ yr. Even if we assume that after one cooling time a steady shock is still non-radiative, the non-radiative region behind the steady shock will extend for less than 16″, much smaller than required by HRB94. The situation is worse at lower V_S: if it takes 950 yr to go from 190 to 170 km s^{-1}, it takes only 685 yr to go from 150 to 130 km s^{-1}.

The case of the models computed by HRB94 is rather extreme, because they build the post-shock structure up to a column density $N_H = 6{\times}10^{17}$ cm^{-2}, corresponding to $t_i \sim 900$ yr for $V_S = 180$ km s^{-1}. Other authors (L92; Blair et al. 1999; Sankrit et al. 2000) use, for the same filament, $t_i \leq 200$ yr. They also suggest that the shock might have recently decelerated. If we examine the time evolution of the shock velocity in the first 200 yr after the shock entered the cloud, we find that during this lapse of time V_S decreased by 16% (from 225 to 189 km s^{-1}) and the post-shock temperature by 30%. As can be seen in Fig. 1, after a few hundred years the $V_S(t)$ distribution becomes flatter, and variations over 200 yr intervals are ≤3% for about a thousand years. Afterwards, the distribution again steepens, and V_S becomes too low (<170 km s^{-1}). At this point, the shock and the NRF are ~15″ further away than the X-ray emitting cavity.

This means that the shock cannot be considered approximately steady for the time necessary to develop a non-radiative region of the size computed by HRB94. It might be approximately steady (variations of 2−3% in V_S and 5−6% in temperature) in the case of the other steady-state non-radiative models cited above, but on the condition that the filament be well inside the cloud and detached (up to 15″) from the X-ray emitting region. One could ask at this point why all the models fitting the emission of the same filament (the one studied by L92) converge on the same shock velocity (170–180 km s^{-1}), even if one of them is certainly not steady, and all the others can be approximately steady, in some particular cases. The only indication that we have is that when the lines are formed closer to the shock, the post-shock region that we have to consider is thinner, and the approximation of the steady-state is more accurate.

The second consequence of the decrease in V_S with time after hitting the wall is that in the reference HD model the development of the shock-wall region is slower than in a steady shock flow. This is because the evolution of the steady shock flow is computed without downstream boundary conditions. In the HD reference model, matter shocked at a given time collides with a pre-existing structure where matter was shocked at higher velocities, because V_S decreases with time. Thus, the shock-wall gap widens at a rate that is slower than in a steady flow. As V_S continues to decrease, there will be a moment when the width of the gap stops growing and begins to decrease. The situation is illustrated in Fig. 3, where we show the time evolution of the size d_{WS} of the region between the shock and the shocked wall of the cavity, as computed with the HD reference model. The dot-dashed straight line indicates the case of a steady shock with $V_S = 180$ km s^{-1}. The HD reference model tells us that the maximum size of the shock-wall region is at most ~25″, because the wall is catching up to the shock.

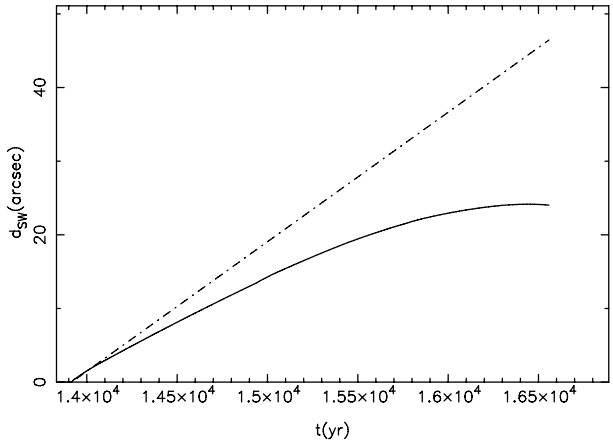

Fig. 3. Time evolution of the width d_{WS} of the region between the shock and the wall of the cavity, as computed in the reference model. The dot-dashed line indicates the evolution of d_{WS} for a steady shock with $V_S = 180\,\mathrm{km\,s^{-1}}$.

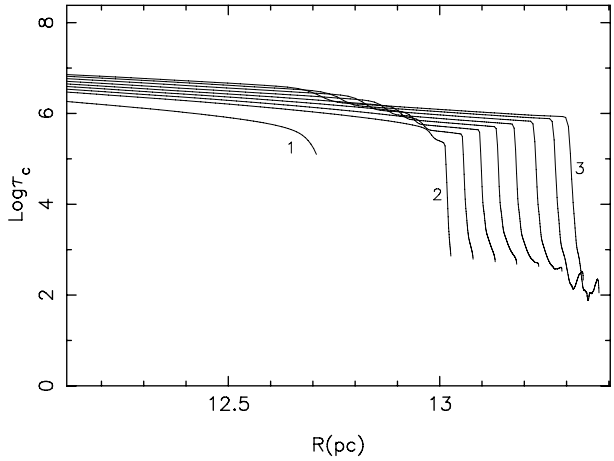

Fig. 4. The radial distribution of the cooling timescale τ_c (in yr) in the reference model. Different evolutionary times are labeled as in Fig. 2.

3.3. Where will radiative cooling take place?

The third parameter that may need revision is one related to the location of the region from which optical radiative emission originates. Observationally, the limit of the presence of [O III] or [S II] optical filaments is roughly coincident with the limit of the hot (>0.2 keV) X-ray emission. The Balmer-dominated region and then the (primary) shock lie beyond this limit. This is clearly shown by Danforth et al. (2000, see their Figs. 4 and 5) who compared multi-wavelength imagery of the NE sector of the Cygnus Loop.

It is believed (see for instance Levenson et al. 1998) that the radial position of the optical emission is most successfully explained by a projection effect: it is probably in the far side of the remnant, while the NRFs are in the near side. Falle & Garlick (1982) built a 2-D HD model based on this geometry. In the following, we examine when and where the HD model predicts the formation of a radiative cooling region.

The possible origins of the optical emission can only be, in order of increasing radius: (*i*) behind the wall of the cavity, (*ii*) in front of the wall, or (*iii*) just behind the shock.

The possibility that optical [O III] or [S II] emission comes from location (*i*) has to be ruled out. In the reference scenario, the interior of the cavity is a low-density, high-temperature environment, where the elements are too ionized to be responsible for that emission. Moreover, the cooling time τ_c is longer than the age of the remnant. This is clearly shown in Fig. 4: in the cavity, even in the region closer to the wall, $\tau_c > 10^5$ yr. On the other hand, one could argue that a dense shell of pre-shocked matter placed in the cavity in the vicinity of the wall could evolve, if the cooling time is low enough, into a radiative region. To test this possibility, we tested a number of models with shells of different densities placed at an initial radius of 12 pc. The results show that indeed the inserted shell can become radiative, if its density is $\geq n_c$. However the parameters of the outer shell/cloud then have to be drastically modified if we still require a primary shock velocity on the order of $180\,\mathrm{km\,s^{-1}}$. In other words, inserting a shell at a smaller radius with roughly the same parameters than the original shell/cloud is equivalent to reducing the scale of the reference scenario (in the tested case, by a factor 12/13).

In the reference model, according to the values of τ_c shown in Fig. 4, the only region where radiative cooling can take place is the one between the wall and the shock. At the time the integration stopped (~2700 yr after hitting the wall), a radiative shell with a peak density of $\geq 10\ \mathrm{cm^{-3}}$ has indeed already developed, with a cooling time ≤ 100 yr. We note that there is practically no gap between the shock and the cooling shell.

3.4. A revised model

The discussion in the preceding sections shows that the test performed with the HD reference model is not entirely satisfactory. A hypothetical "reference model" Cygnus Loop would (*i*) appear hotter in X-rays, (*ii*) have a shock velocity that decreases rather rapidly and falls below the observed values ~1100 yr after hitting the cloud, and (*iii*) have optical filaments that develop just behind the shock.

We choose to revise the basic parameters of the reference model to assure an acceptable steadiness of the shock velocity in the range $180 \pm 10\ \mathrm{km\,s^{-1}}$, from the crossing of the wall to the time of observation. This does not imply that the flow will be steady. To ensure that V_S remains approximately in this range, the density of the cloud should not be constant, but decrease with radius. We found that fixing the parameter $a = a^+ = 0.5$ in Eq. (1) produces approximately a constant $V_S(r)$ (see Fig. 5).

From 21 cm observations of the NE sector of the Cygnus Loop, Leahy (2003) conclude that a partial shell of atomic hydrogen is adjacent to the NE limb of the remnant. The density in this region seems to be higher than that presently experienced by the shock, and to increase at larger radii. This picture is not in contrast with the suggestion that there is a density decrease after the wall: the H I cloud is not yet in contact with the shock, and the proposed decrease may just be local.

We have seen in Sect. 3.1 that to be certain that the temperature distribution in the cavity is in the range observed (0.2–0.3 keV), the assumed velocity at the moment the shock hits the wall has to be lower than $400\,\mathrm{km\,s^{-1}}$. As can be seen in Fig. 6, the lower V_S at the moment the shock hits the wall generates a weaker reflected wave. Already shocked matter in the cavity is then compressed and heated to temperatures in the observed range. We also finely adjusted other parameters such as the density contrast at the cavity-cloud interface, and the pre-shocked radius of the interface. The input parameters used in the revised model are showed in the third column of Table 1.

One may ask why we modified the density profile of the cloud to maintain an almost constant V_S, if models more recent than that of HRB94 are reasonably steady even for the

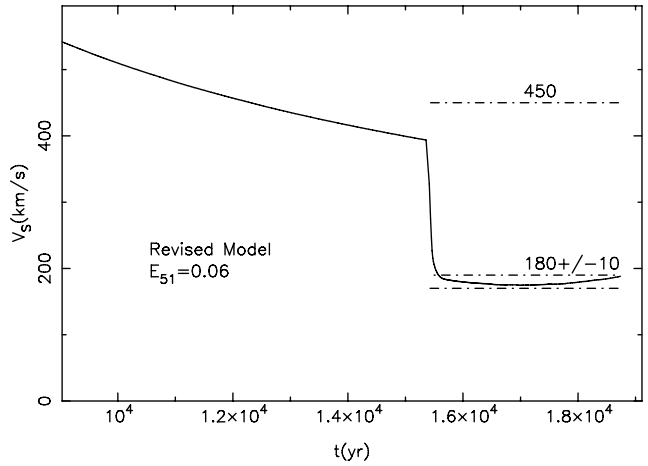

Fig. 5. Time evolution of the shock velocity V_S in the revised model ($E_{51} = 0.06$). Dot-dashed lines are drawn at $V_S = 180 \pm 10$ and 450 km s^{-1}.

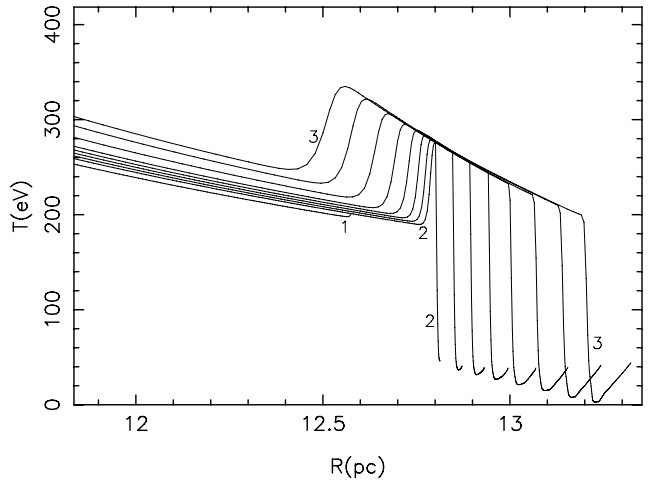

Fig. 6. The radial temperature distribution (T in eV) in the revised model at different times before and after hitting the cavity wall. Labels 1 to 3 refer to the specific times: (1) −670 yr, (2) +120 yr, (3) +3300 yr.

parameters of the reference model. Why is a reduction in the explosion energy not enough? The point is that the reduction in the explosion energy alone will indeed generate a post-shock structure re-heated by the reflected compression wave at the observed temperatures, but at the same time the shock velocity will fall below the observed value(s). To recover a V_S in the range of 180 ± 10 km s^{-1}, we should decrease the (constant) density of the cloud below the observed values of 1–2 cm^{-3}. The choice of the parameters of the revised model is then a reasonable compromise imposed by different constraints.

As in the reference model, the only region in the revised model where radiative cooling can take place is the one between the wall and the shock. At the end of the integration, ~3300 yr after hitting the wall, a dense ($n > 25$ cm^{-3}) recombining shell rapidly forms. However this time the cooling region is much closer to the wall than to the shock. The gap between the shock and the optical filaments is on the order of 30″ at the end of the integration.

Table 2. Determinations of the explosion energy.

Author	E_{51}	E_{51}@540 pc
Rappaport et al. (1974)	0.3 (d/770)^3	0.1
Braun & Strom (1986)	0.75 (d/460)^3	1.21
	0.18 (d/460)^3	0.3
Miyata & Tsunemi (1999)	0.3 (d/770)^3	0.1
This work:		
Reference model	0.08 (d/540)^3	0.08
Revised model	0.06 (d/540)^3	0.06

3.5. The Cygnus Loop SN

Not many authors in the past have evaluated the explosion energy of the Cygnus Loop SN. In Table 2, we list the authors, the explosion energies (in units of 10^{51} erg), and the distances used, and in the last column the values of the energy normalized to the distance adopted in the present paper (540 pc; Blair et al. 2005).

The value of E_{51} that we find is actually very low, although consistent with the value found by Miyata & Tsunemi (1999), once their value is scaled to the smaller distance used in the present paper. The value of E_{51} depends on the distance d as $(d/540\ \mathrm{pc})^3$, so we could recover a more standard $E_{51} \simeq 1$ by placing the remnant at $d \simeq 1250$ pc. This distance is well outside the range (460–770 pc) found by authors (Braun & Strom 1986; Minkowski 1958) that did not use a steady-shock analysis to derive the space velocity of the shock, and a factor of 2 higher than the recent upper limit to the distance found by Blair et al. (2009).

Since the work of HRB94, other estimates of the density n_0 of the pre-shocked medium seems to indicate a higher n_0, on the order of 0.2 cm^{-3} or above (Raymond et al. 2003; Sankrit et al. 2010). If we use for the distance the upper limit of 640 pc (Blair et al. 2005, 2009) and assume that $n_0 = 0.2$ cm^{-3}, we derive for E_{51} the upper limits of 0.26 and 0.20 for the reference and revised model, respectively. We can derive another upper limit for E_{51} assuming that all the shocked mass inside the cavity (with pre-shocked density n_0) is concentrated in a very thin shell at radius R_w, and that the particle velocity is constant and equal to its maximum value of $u = 3/4 V_S$, where V_S is the value of the shock velocity just before hitting the wall. Assuming again a self-similar adiabatic structure, where the kinetic energy is about 28% of the total energy, we find that $E_{51} < 0.13$ and $E_{51} < 0.09$ for the reference and the revised model, respectively. If we assume that $n_0 = 0.2$ cm^{-3}, the above estimates become $E_{51} < 0.26$ and $E_{51} < 0.18$. Using as upper limit for E_{51} the highest value derived above and for lower limit the value obtained placing the revised model at the lowest value of the distance (300 pc; Braun & Strom 1986) we get $0.01 < E_{51} < 0.26$.

From their observations of the NE limb with *ASCA*, Miyata & Tsunemi (1999) estimate an explosion energy $E_{51} \simeq 0.3$ (at 770 pc), a total mass of the ejecta of 4.1 $M_\odot$ and a main-sequence mass of the progenitor star of ~15 $M_\odot$. The low explosion energy found in the present work – and in previous works once E_{51} is scaled to the distance of 540 pc – suggests that the progenitor of the SN of the Cygnus Loop was probably a star near the lower end of the mass range of core-collapse SN progenitors, i.e. a star with a mass of ~8–10 $M_\odot$, which fits naturally an electron-capture SN explosion scenario (Nomoto 1984). Simulations of SN explosions from the collapse of degenerates O-Ne-Mg cores compiled by Kitaura et al. (2006) indeed demonstrated that these events have explosion energies on the order of $\sim 0.1 \times 10^{51}$ erg. The Cygnus Loop SN was then probably similar to SN 2005cs, a

sub-luminous type II-P in M51 with $E_0 \sim 3{\times}10^{50}$ erg (Pastorello et al. 2009), or to the faint type Ib SN 2005E (Perets et al. 2010).

A point that should be investigated though is how a progenitor of ~8–10 $M_\odot$, with a spectral type B, can generate a cavity such as that of the Cygnus Loop. Alternatively, one could ask the question do we really need a cavity? In brief, the reasons for considering a cavity-wall scenario are: (i) the co-existence of low-V_S NRFs with hot matter; and (ii) the morphology of the X-ray emission and the strong limb-brightening (see for instance Levenson et al. 1997). Although the former remains applicable, the latter should be investigated further.

In the future, we should also evaluate the effect of a weaker injection of energy from stars in this mass interval on models of galactic evolution.

In our Galaxy, the Crab SN has also been considered the result of the core-collapse explosion of a low-mass progenitor (Fesen et al. 1997), with the expansion velocity of the filaments representing a kinetic energy on the order of $0.6–1.5 \times 10^{50}$ erg. However, the explosion energy of the Crab SN is estimated to be in the range $0.5–2{\times}10^{51}$ erg (Davidson & Fesen 1985). With an estimated $E_0 \simeq 6 - 8 \times 10^{49}$ erg, and the above upper and lower limits, the Cygnus Loop is the result of the weakest known core-collapse SN in our Galaxy.

4. Conclusions

The current hypothesis is that the Cygnus Loop SN exploded within a cavity formed by the wind of the progenitor star. After crossing the cavity, the shock hit the cavity wall and is now running through a denser environment (a cloud). In this work, we have tested the consistency of the global parameters of the remnant (as derived at the cavity-cloud interface assumed to be a discontinuity) with the observational scenario in the NE sector of the remnant. A 1-D spherically symmetric HD code has been used to develop a model through the wall of the cavity into the cloud, using a smooth density distribution at the cavity-cloud interface.

As the main shock hits the wall of the cavity, we have found that the reflected perturbation is not a shock but a strong compression wave. We have tested different slopes and different density jumps for the density distribution of the wall, but the resulting reflected perturbation is always a compression wave. A reflected shock is generated only in the case of a discontinuity in the density distribution.

In the reference model of the cavity-wall scenario, after crossing the wall of the cavity, the shock velocity rapidly reaches values in the observed range of $V_S = 180 \pm 10$ km s^{-1}, but then continues to decrease, V_S falling below this range ~1100 yr after the crossing of the wall. This may be a problem for determinations of V_S using steady-state shock models. Models that build-up their post-shock structure for $t_i > 200$ yr, or assume that the shock has hit the cloud and decelerated in the recent past (<200 yr ago) cannot be considered steady. In contrast, the steady-state approximation may be rather good (V_S variations ≤3%) for models with narrower post-shock structures (i.e. $t_i < 200$ yr) and a cloud that was shocked 200–1100 yr ago.

In the reference model, the temperature decreases outwards as indicated by X-ray observations, but the model cannot reproduce the extent of the region where this occurs, even if we allow the reflected wave to reheat the cavity long enough for radiative cooling to appear in the shocked cloud. We also find that the use of the X-ray observed plasma temperatures to infer the value of the shock velocity just before hitting the wall of the cavity generates a model with a temperature radial profile well above the observed values. This is because a reflected compression wave heats the already shocked plasma in the cavity to even higher temperatures.

We have computed a model with revised values for the parameters of the cavity-wall scenario, assuming as a constraint the approximate steadiness of the shock velocity. This does not mean that the shock is steady, because the steadiness of the shock velocity is obtained at the expense of a variable pre-shock ambient density. In the revised model, we have found that: (*i*) the shock velocity is consistent with the value derived with the steady-state analysis of L92, HRB94, and Blair et al. (1999), and this over a much longer evolutionary time; (*ii*) the temperature distribution of the hot matter close to the wall of the cavity is well within the range observed in the X-ray, although not over the same radial extent. Additional work is needed to clarify this point, both for the X-ray derived temperature distribution and the parameters of the cavity-wall scenario.

As for the position of radiative regions, we note that although the bright, optical radiative filaments observed in the remnant are currently explained as being on the far side of the remnant, with the NRFs being on the near side, the models do predict the appearance of a radiative region 3–4000 yr after the shock entered the cloud. We have shown that changing the input parameters of the models (from the reference to the revised model) we can move the location of the radiative region from the classical position just behind the shock to a position close to the border of the cloud.

As a byproduct of the computations performed above (i.e., from the initial conditions of the HD models), we have found an explosion energy of $E_0 \simeq 6–8 \times 10^{49}$ erg – consistent with previous determinations, once scaled to the distance adopted in the present paper – with an upper limit of 2.6×10^{50} erg (distance 640 pc, $n_0 = 0.2$ cm^{-3}) and a lower limit of 0.1×10^{50} erg (distance 300 pc, $n_0 = 0.09$ cm^{-3}). Any one of these values implies that the SN of the Cygnus Loop is the weakest known core-collapse SN in the Galaxy.

Acknowledgements. We thank two anonymous referees for their valuable and stimulating comments.

References

Blair, W. P., Sankrit, R., Raymond, J. C., & Long, K. S. 1999, AJ, 118, 942
Blair, W. P., Sankrit, R., & Raymond, J. C. 2005, AJ, 129, 2268
Blair, W. P., Sankrit, R., Torres, S. I., Chayer, P., & Danforth, C. W. 2009, ApJ, 692, 335
Braun, R., & Strom, R. G. 1986, A&A, 164, 208
Cox, D. P. 1972, ApJ, 178, 143
Danforth, C. W., Cornett, R. H., Levenson, N. A., Blair, W. P., & Stecher, T. P. 2000, AJ, 119, 2319
Davidson, K., & Fesen, R. A. 1985, ARA&A, 23, 119
Dere, K. P., Landi, E., Mason, H. E., Monsignori Fossi, B. C., & Young, P. R. 1997, A&AS, 125, 149
Dwarkadas, V. V. 2005, ApJ, 630, 892
Dwarkadas, V. V. 2007, ApJ, 667, 226
Falle, S. A. E. G. 1975, MNRAS, 172, 55
Falle, S. A. E. G., & Garlick, A. R. 1982, MNRAS, 201, 635
Fesen, R. A., Shull, J. M., & Hurford, A. P. 1997, AJ, 113, 354
Fusco-Femiano, R., & Preite-Martinez, A. 1984, ApJ, 281, 593
Hester, J. J., Raymond, J. C., & Blair, W. P. 1994, ApJ, 420, 721
Katsuda, S., & Tsunemi, H. 2008, Adv. Space Res., 41, 383
Katsuda, S., Tsunemi, H., Kimura, M., & Mori, K. 2008a, ApJ, 680, 1198
Katsuda, S., Tsunemi, H., Uchida, H., et al. 2008b, PASJ, 60, 115
Kitaura, F. S., Janka, H., & Hillebrandt, W. 2006, A&A, 450, 345
Leahy, D. A. 2003, ApJ, 586, 224
Levenson, N. A., Graham, J. R., Aschenbach, B., et al. 1997, ApJ, 484, 304
Levenson, N. A., Graham, J. R., Keller, L. D., & Richter, M. J. 1998, ApJS, 118, 541

Levenson, N. A., Graham, J. R., & Walters, J. L. 2002, ApJ, 576, 798
Long, K. S., Blair, W. P., Vancura, O., et al. 1992, ApJ, 400, 214
McCray, R., & Snow, Jr., T. P. 1979, ARA&A, 17, 213
Minkowski, R. 1958, Rev. Mod. Phys., 30, 1048
Miyata, E., & Tsunemi, H. 1999, ApJ, 525, 305
Miyata, E., & Tsunemi, H. 2001, ApJ, 552, 624
Miyata, E., Katsuda, S., Tsunemi, H., Hughes, J. P., Kokubun, M., & Porter, F. S. 2007, PASJ, 59, 163
Nemes, N., Tsunemi, H., & Miyata, E. 2008, ApJ, 675, 1293
Nomoto, K. 1984, ApJ, 277, 791
Pastorello, A., Valenti, S., Zampieri, L., et al. 2009, MNRAS, 394, 2266
Perets, H. B., Gal-Yam, A., Mazzali, P. A., et al. 2010, Nature, 465, 322
Preite-Martinez, A. 1981, A&A, 96, 283
Preite Martinez, A. 2009, The Open Astronomy Journal, 2, 1
Rappaport, S., Doxsey, R., Solinger, A., & Borken, R. 1974, ApJ, 194, 329
Raymond, J. C. 1979, ApJS, 39, 1
Raymond, J. C., Blair, W. P., Fesen, R. A., & Gull, T. R. 1983, ApJ, 275, 636
Raymond, J. C., Ghavamian, P., Sankrit, R., Blair, W. P., & Curiel, S. 2003, ApJ, 584, 770
Sankrit, R., Blair, W. P., Raymond, J. C., & Long, K. S. 2000, AJ, 120, 1925
Sankrit, R., Williams, B. J., Borkowski, K. J., et al. 2010, ApJ, 712, 1092
Sedov, L. I. 1959, Similarity and Dimensional Methods in Mechanics, ed. L. I. Sedov
Uchida, H., Tsunemi, H., Katsuda, S., et al. 2009, ApJ, 705, 1152